

Weak coupling renormalization-group analysis of two-dimensional Hubbard models: application to high- T_c and $\kappa - (BEDT - TTF)_2X$ organic superconductors

Shan-Wen Tsai* and J. B. Marston

Department of Physics, Brown University, Providence, RI 02912-1843

(February 5, 2020)

We present a weak coupling renormalization-group analysis of the Hubbard model on the anisotropic triangular lattice. As the model interpolates between the nearest-neighbor square lattice and decoupled chains via the isotropic triangular lattice, it permits the study of competition between antiferromagnetic and BCS Cooper instabilities. We begin by reproducing known results for decoupled chains, and for the square lattice with only nearest-neighbor hopping amplitude t_1 . We examine both repulsive and attractive Hubbard interactions. The role of formally irrelevant contributions to the one-loop renormalization-group flows is also studied, and these subleading contributions are shown to be important in some instances. We then demonstrate that crossover to a BCS-dominated regime can occur even at half-filling when antiferromagnetism is frustrated through the introduction of a next-nearest-neighbor hopping amplitude t_2 along one of the two diagonal directions. The resulting anisotropic triangular lattice may describe the conducting layers of the organic $\kappa - (BEDT - TTF)_2X$ materials. Stripes are not expected to occur and time-reversal breaking $d_{x^2-y^2} \pm id_{xy}$ superconducting order does not arise spontaneously; instead pure $d_{x^2-y^2}$ order is favored. At the isotropic triangular point ($t_1 = t_2$) we find the possibility of re-entrant antiferromagnetic long-range order.

PACS numbers: 74.20.Mn, 74.25.Dw, 74.70.Kn, 71.10.Fd

I. INTRODUCTION

Intriguing experiments¹⁻³ on the $\kappa - (BEDT - TTF)_2X$ family of layered organic molecular crystals have evoked comparison with similar experiments with high-temperature superconductors. The layered organic materials exhibit a wide variety of electronic properties. In particular, the phase diagram is rather similar to that of the high- T_c cuprates⁴ and there is some evidence for unconventional pairing with nodes in the gap from NMR relaxation rate^{5,6}, specific heat⁷ and penetration depth^{8,9} measurements. Other experiments, however, suggest *s*-wave pairing¹⁰⁻¹³. Competition between antiferromagnetic and superconducting instabilities, seen in the cuprates, also seems to occur in the $\kappa - (BEDT - TTF)_2X$ compounds¹⁴.

The Hubbard model on the anisotropic triangular lattice was proposed by McKenzie⁴ as a model of the conducting layers of $\kappa - (BEDT - TTF)_2X$. It is a simplified version of a model first introduced by Kino and Fukuyama¹⁵. Two hopping matrix elements are introduced and the Hamiltonian is given by:

$$H = -t_1 \sum_{\langle ij \rangle} (c_i^{\dagger\sigma} c_{j\sigma} + H.c.) - t_2 \sum_{\langle\langle ij \rangle\rangle} (c_i^{\dagger\sigma} c_{j\sigma} + H.c.) + U \sum_i n_{i\uparrow} n_{i\downarrow} - \mu \sum_i n_i, \quad (1)$$

where $\langle ij \rangle$ denotes nearest-neighbor pairs of sites on the square lattice and $\langle\langle ij \rangle\rangle$ denotes next-nearest-neighbor pairs along one of the two diagonal directions of the square lattice as shown in Fig. 1. Quantum chemistry calculations suggest that, in contrast to the cuprate materials, in the case of the organic $\kappa - (BEDT - TTF)_2X$ compounds the Hubbard interaction $U \approx t$. Thus a weak-coupling renormalization-group (RG) approach such as we adopt here is reasonable.

*new address: Department of Physics, University of Florida, Gainesville, FL 32611-8440 (tsai@phys.ufl.edu)

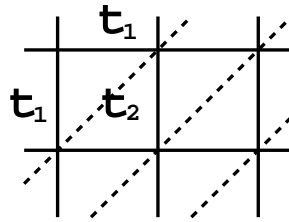


FIG. 1. Anisotropic triangular lattice with two hopping amplitudes t_1 and t_2 . The limit $t_2 = 0.0$ corresponds to the usual nearest-neighbor square lattice and $t_1 = 0.0$ corresponds to decoupled chains.

The model is also interesting in its own right as it interpolates between the square lattice and decoupled chains. At half-filling, the non-interacting Fermi surface is perfectly nested in these two extreme limits. As nesting is imperfect in between the limiting cases, several phase transitions can be expected. The square lattice, which has been the subject of many studies, corresponds to the special case of zero next-nearest-neighbor hopping, $t_2 = 0$. When the repulsive interaction is turned on, nesting induces a spin density wave instability. In the opposite limit, $t_1 = 0$, the chains are completely decoupled. These isolated chains have no spin order and are described by the exact Bethe ansatz solution of Lieb and Wu¹⁶. We pay particular attention to the intermediate region of $t_1 \neq 0$ and $t_2 \neq 0$ and study it via a weak-coupling renormalization-group analysis. The special isotropic triangular lattice point corresponds to $t_1 = t_2$. Values for the hopping matrix elements obtained from experiments and from quantum chemistry calculations for the conducting layer of $\kappa - (BEDT - TTF)_2X$ suggest $t_1 > t_2$, that is, somewhere intermediate between the square and the isotropic triangular limits. The lattice anisotropy can be altered by uniaxial stress applied along the principal axes of the quasi-two-dimensional organic compound¹⁷. Fermi surfaces of non-interacting electrons for different ratios of the hopping matrix elements are shown in Fig. 2.

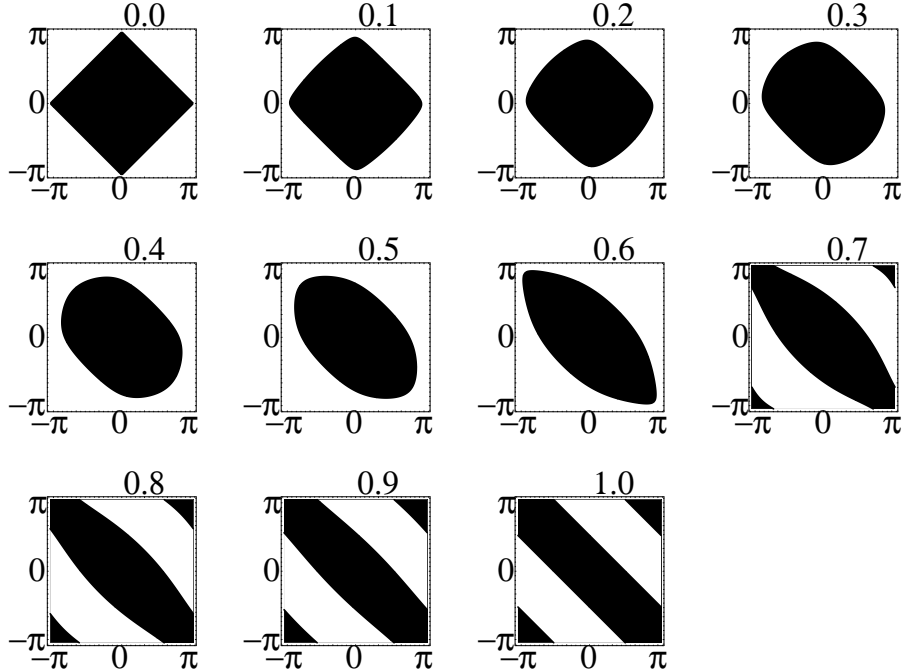


FIG. 2. Fermi surface of non-interacting electrons for different ratios of the two hopping amplitudes. The number at the top of each graph is the anisotropy ratio $t_2/(t_1 + t_2)$ which ranges from 0 (square lattice) to 1 (decoupled chains). The chemical potential μ is varied to ensure that the system is always half-filled.

In the next section we briefly introduce the RG method we employ, a method first implemented by Zanchi and Schulz¹⁸ for the square lattice. We then present results of our calculations at different values of the anisotropy: decoupled chains (studied as a test case to check the reliability of the calculation), square lattice, and finally the anisotropic region intermediate between the square lattice and the isotropic triangular lattice. We discuss the ordering tendencies and work out the implied phase diagram as a function of anisotropy parameter $t_2/(t_1 + t_2)$ which ranges from 0 (square lattice) to 1 (decoupled chains). We also make comparison to results in the strong-coupling limit of

large on-site repulsion obtained via other methods.

II. RENORMALIZATION-GROUP CALCULATION

We follow the weak-coupling renormalization-group analysis implemented by Zanchi and Schulz¹⁸ for interacting fermions on a two-dimensional lattice. Like some previous work¹⁹, the approach generalizes Shankar's renormalization group theory²⁰ to Fermi surfaces of arbitrary shape. More significantly, in principle the *only* approximation that is made in the approach of Zanchi and Schulz is an expansion in powers of the interaction strength, the on-site Coulomb interaction U . Subleading terms generated during the RG transformations, which are dropped as irrelevant in the simplest versions of the RG, are instead kept in this formulation. Specifically, the formally irrelevant, non-logarithmic, terms which appear in the six-point function during the process of mode elimination do in fact contribute to the RG flows. Thus while the simplest weak-coupling RG analyses makes a double expansion in both the interaction strength and in the relevance of the terms retained in the renormalization flows, in the approach of Zanchi and Schulz there is only a single expansion in the interaction strength. (In practice some added approximations are made for computational convenience, as detailed below. These simplifications are not expected to alter the results significantly.) As we show below, in some cases this more accurate treatment leads to substantial differences in the RG flows.

Elimination of high energy modes is carried out iteratively, in infinitesimal steps, and as a result the energy cutoff Λ around the Fermi surface shrinks, see Fig. 3. The initial energy cutoff is taken to be the full band width Λ_0 , and it is reduced via continuous mode elimination to $\Lambda = \Lambda_0 e^{-\ell}$ where $\ell > 0$.

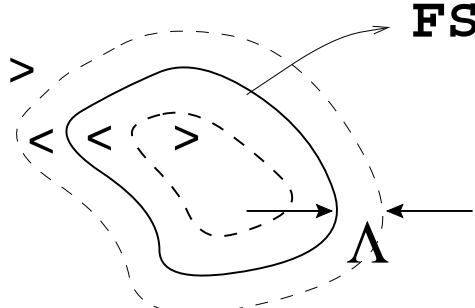


FIG. 3. Mode elimination is carried out in infinitesimal steps. The figure shows the low energy modes (denoted $<$) which are inside a shell of thickness Λ around the Fermi surface, and the high energy modes, which have already been integrated out and which are now outside the shell. At each step the on-shell modes precisely at scaling parameter ℓ (dashed lines) are integrated out.

For each infinitesimal step $\ell \rightarrow \ell + d\ell$, the fermion degrees of freedom are broken down into high and low energy modes as

$$\Psi_\sigma(K) = \Theta(\Lambda - |\epsilon_{\mathbf{k}}|) \Psi_{\sigma,<}(K) + \Theta(|\epsilon_{\mathbf{k}}| - \Lambda) \Psi_{\sigma,>}(K), \quad (2)$$

where $K \equiv (\omega, \mathbf{k})$ is the usual 2+1-dimensional frequency-momentum vector. The effective action, after dropping a constant contribution $\Omega_>$ to the free energy, has the form

$$S_{\Lambda(\ell+d\ell)} = S_{\Lambda(\ell)} + \delta S(\ell). \quad (3)$$

At non-zero $\ell > 0$ the effective action contains contributions at all orders in the initial interaction strength. But because mode elimination is done in infinitesimal steps, only terms linear in $d\ell$ contribute to $\delta S(\ell)$. These terms correspond to diagrams with one internal line (either a loop or a tree diagram). RG flow equations for vertices with any number of legs, $\Gamma_{2n}(\ell)$, can then be found. These are functional equations since the Γ 's are functions of momenta and frequencies.

To make progress we must make an approximation. We carry out the weak-coupling expansion by truncating the RG equations at the one-loop level. Renormalization of the effective interaction $U_\ell(\mathbf{k}_1, \mathbf{k}_2, \mathbf{k}_3, \mathbf{k}_4)$, corresponding to the four-point function (Γ_4), then occurs at order U^2 . Contributions from the six-point functions Γ_6 must also be included at this order. Higher n-point functions may be neglected as these only contribute at higher-order in the interaction strength U . It is important to notice that the RG flow equations generated this way are non-local in scaling parameter ℓ . The RG equations for couplings $U_\ell(\mathbf{k}_1, \mathbf{k}_2, \mathbf{k}_3, \mathbf{k}_4)$ at step ℓ involve the values of couplings at previous steps ℓ_{pp} and ℓ_{ph} [the subscript denotes particle-particle (pp) and particle-hole (ph) channels]:

$$\ell_{pp} = -\ln \left(\frac{\epsilon_{\mathbf{k}-\mathbf{q}_{pp}}}{\Lambda_0} \right) \quad (4)$$

$$\ell_{ph} = -\ln \left(\frac{\epsilon_{\mathbf{k}+\mathbf{q}_{ph}}}{\Lambda_0} \right) \quad (5)$$

with $\mathbf{q}_{pp} = \mathbf{k}_1 + \mathbf{k}_2$ and $\mathbf{q}_{ph} = \mathbf{k}_1 - \mathbf{k}_4$. At step ℓ contributions from six-point functions are obtained by contracting two of the legs at on-shell momentum \mathbf{k} . Of course the six-point functions were generated from four-point functions during previous steps. Momentum \mathbf{k}_4 is also set by momentum conservation to be $\mathbf{k}_4 = \mathbf{k}_1 + \mathbf{k}_2 - \mathbf{k}_3$.

For an initial four-fermion interaction U_0 which is independent of spin, following Zanchi and Schulz, it is possible¹⁸ to write all the renormalized two-particle interactions in terms of only one function $U_\ell(\mathbf{k}_1, \mathbf{k}_2, \mathbf{k}_3)$. Couplings in the charge and spin sectors can then be obtained from this function through the relations:

$$U_c = \frac{1}{4}(2 - \hat{X})U, \quad U_\sigma = -\frac{\hat{X}}{4}U. \quad (6)$$

where \hat{X} is a permutation operator defined by its action: $\hat{X}U(\mathbf{k}_1, \mathbf{k}_2, \mathbf{k}_3) \equiv U(\mathbf{k}_2, \mathbf{k}_1, \mathbf{k}_3)$. The spin coupling and the charge-density-wave (CDW) coupling are then given by

$$\begin{aligned} V_\ell^{AF}(\theta_1, \theta_2) &= 4U_{\sigma\ell}(\mathbf{k}_1, \mathbf{k}_2, \tilde{\mathbf{k}}_1) \\ V_\ell^{CDW}(\theta_1, \theta_2) &= 4U_{c\ell}(\mathbf{k}_1, \mathbf{k}_2, \tilde{\mathbf{k}}_1) . \end{aligned} \quad (7)$$

Here $\tilde{\mathbf{k}}$ is obtained from \mathbf{k} by the relation $\mathbf{k} - \tilde{\mathbf{k}} = \mathbf{Q}$ where \mathbf{Q} is a nesting vector ($\mathbf{Q} = (\pm\pi, \pm\pi)$ for the fully nested square lattice). Forward and BCS scattering amplitudes are given by

$$\begin{aligned} F_\ell(\theta_1, \theta_2) &= U_\ell(\mathbf{k}_1, \mathbf{k}_2, \mathbf{k}_1) \\ V_\ell^{BCS}(\theta_1, \theta_2) &= U_\ell(\mathbf{k}_1, -\mathbf{k}_1, \mathbf{k}_2) . \end{aligned} \quad (8)$$

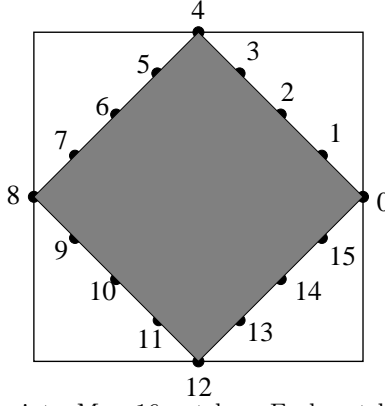


FIG. 4. Discretization of the Fermi surface into $M = 16$ patches. Each patch corresponds to an angular section of $2\pi/M$. The special case of the perfectly-nested Fermi surface corresponding to the nearest-neighbor tight-binding model on a square lattice and at half-filling is shown.

In order to integrate the flow equations forward in the scaling parameter ℓ we first discretize the Fermi surface, dividing it up into patches as depicted in Fig. 4. Interactions $U_\ell(i_1, i_2, i_3)$ are thus labeled by three discrete patch indices. A fourth patch index i_4 is determined from momentum conservation. A further approximation is implied by this procedure, as the dependence of the effective interaction on the radial component of momentum is neglected and the shape of the Fermi surface is not renormalized. The justification is the following: though the shape of the Fermi surface change at the one-loop level, the feedback of this change on the one-loop RG flows for the couplings $U_\ell(i_1, i_2, i_3)$ constitutes a higher-order effect. The dependence of U on the radial components of the three momenta is irrelevant^{21,20}. This is similar to the one-dimensional case, where the marginal interactions are labeled according to the indices $i = R, L$ (right or left moving) of the electrons in the interaction. There is strong dependence on the direction of \mathbf{k} , but the dependence on the absolute value k of the momentum is irrelevant. Therefore the interactions may be parameterized simply by their projection onto the two Fermi points. In two dimensions the interactions are likewise parameterized by the patch indices.

In this work we only study flows at zero temperature. The integral over Matsubara frequencies, which arises in the one-loop diagram, can be performed analytically as the dependence of the couplings on the frequency ω is irrelevant²¹. We set the initial bare coupling to be $|U_0| = 4/3$ and, unless otherwise stated, also set $t_1 + t_2 = 1$. We usually divide the Fermi surface into $M = 16$ patches. For the special case of the isotropic triangular lattice we instead use a finer mesh of patches, $M = 24$. Our algorithm makes no assumptions about the symmetries of Fermi surface; this means that we must follow the flow of all M^3 couplings $U(i_1, i_2, i_3)$. We do impose the requirement that the three indices are such that all four particles lie on the Fermi surface. The RG flow for these couplings are then described by coupled non-local integral-differential equations. These equations are numerically integrated forward in the scaling parameter ℓ . The increment in the scaling parameter is set to be $d\ell = 1/9$ for the results shown here. Calculations using smaller values of $d\ell$ yield nearly the same results.

An equivalent version of RG method for two-dimensional interacting fermions has been developed by Salmhofer^{22,23}. In this formulation, the RG flow equations are *local* in the scaling parameter ℓ , but this gain comes at the cost of expanding the effective action in *Wick-ordered* monomials, resulting in RG flow equations with one extra integration over momentum. This formulation has been used to study the two-dimensional Hubbard model on a square lattice with nearest-neighbor and next-nearest-neighbor hopping amplitudes^{24–26}.

III. RESULTS

We now turn to the results of our RG calculation. We first check the method in the special limiting cases of decoupled chains and the pure square lattice. As we reproduce known results in these limits, we then turn to the more general problem of the anisotropic triangular lattice.

A. Decoupled chains ($t_1 = 0$)

As a first check, we apply the weak-coupling analysis to the case $t_1 = 0$ and $t_2 = 1$ which corresponds to completely decoupled chains. At half-filling, particle-hole symmetry requires $\mu = 0$. For repulsive initial interaction ($U_0 > 0$), the antiferromagnetic (AF) couplings decrease towards zero, while Umklapp and charge-density wave interactions diverge in the low-energy limit. This is as expected for a single chain with repulsive Hubbard interaction¹⁶ since the system has gapless spin excitations while the charge sector is gapped. On the other hand, for attractive initial interaction ($U_0 < 0$) the AF couplings diverge while Umklapp and charge-density wave couplings tend towards zero. In this case there is a gap in the spin sector and gapless charge excitations. These two cases are illustrated in Fig. 5.

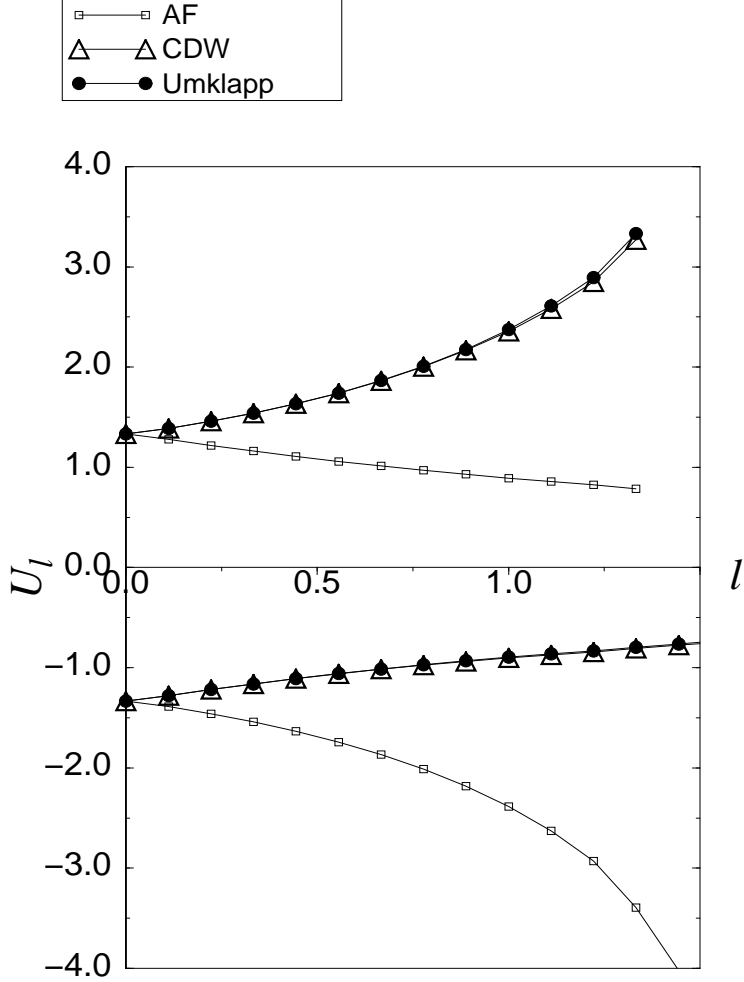


FIG. 5. RG flows of the antiferromagnetic (AF), charge-density wave (CDW) and Umklapp interactions, in the limit of completely decoupled chains ($t_1 = 0$). For repulsive (attractive) bare interaction $U_0 > 0$ ($U_0 < 0$), a charge (spin) gap develops and there are gapless spin (charge) excitations.

B. Square lattice ($t_2 = 0$)

Attractive interactions $U_0 < 0$ induce strong BCS instabilities in the case $t_2 = 0.0$ of a pure square lattice, in accord with expectations. The effective BCS interaction $V_\ell^{BCS}(i_1, i_2)$, as defined by Eq. 8, is a symmetric $M \times M$ matrix in the patch indices and it is useful to diagonalize it. The eigenvector ϕ with the largest attractive eigenvalue then represents the dominant BCS channel. It is plotted in Fig. 6 for the case of half-filling, $\mu = 0$. As expected, the dominant BCS pairing channel is isotropic (that is, s -wave) when $U_0 < 0$. From the outset at $\ell = 0$ the BCS sector dominates all other channels. As the RG flows progress, the BCS channel diverges and thus remains the dominant coupling. The same qualitative behavior persists as the system is doped away from half-filling. We may also calculate the eigenvectors and eigenvalues of the effective spin coupling $V_\ell^{AF}(i_1, i_2)$ to determine the dominant AF channel. Fig. 7 shows the RG flows of the BCS channel (solid line) and the AF channel (dashed line) for the case $\mu = 1$. Also plotted are the results of RG flows with only the leading logarithmic contributions. As the BCS coupling is not driven here by the AF fluctuations, there is little coupling between the two channels. Therefore, one-loop RG flows which include only the leading logarithmic contributions (diamonds) do not differ significantly from the more accurate approach of Zanchi and Schulz (circles) which includes all the subleading non-logarithmic terms.

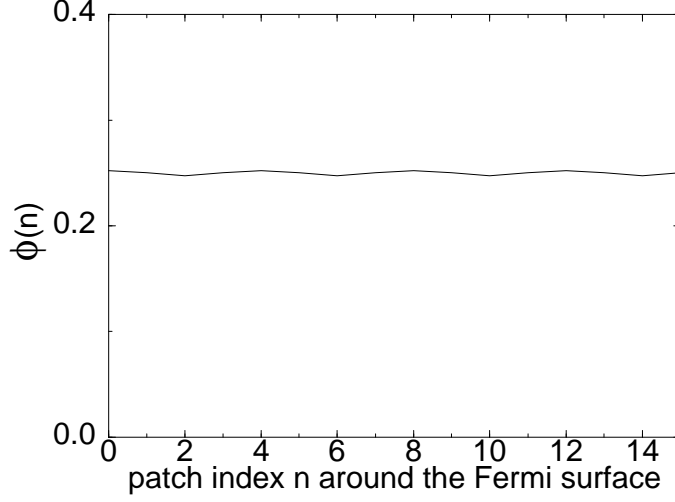


FIG. 6. Pairing symmetry of the dominant BCS channel for the case of attractive initial interaction ($U_0 < 0$) on a square lattice ($t_1 = 1$ and $t_2 = 0$) at half-filling ($\mu = 0$). The Fermi surface is divided in $M = 16$ patches. As the patch index goes from $n = 0$ to $n = 15$ around the Fermi surface, the angle θ goes from 0 to 2π .

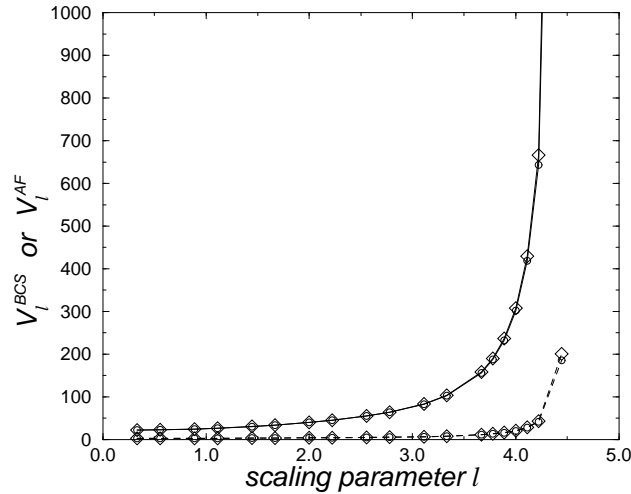


FIG. 7. Comparison of results obtained from the approach of Zanchi and Schulz (circles) with those obtained when only logarithmic contributions are included (diamonds), for the case of an attractive Hubbard interaction ($U_0 < 0$) and $\mu = 1$. There is no significant discrepancy between the results. Flow in the dominant BCS coupling is shown by the solid line; the AF coupling is indicated by the dashed line.

The opposite limit of a square lattice with repulsive initial interaction $U_0 > 0$ has been extensively studied^{18,24}. At half-filling, the Fermi surface is perfectly nested and a strong SDW instability develops. Fig. 8 shows, however, that the largest BCS channel, though sub-leading in comparison to the SDW channel, already exhibits $d_{x^2-y^2}$ pairing symmetry.

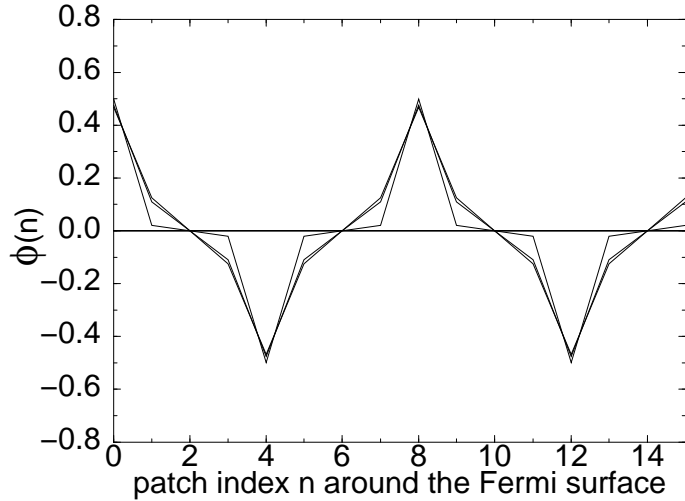


FIG. 8. Pairing symmetry of the dominant BCS channel for the case of repulsive initial interaction ($U_0 > 0$) on the square lattice ($t_1 = 1$ and $t_2 = 0$) at half-filling ($\mu = 0$). The different curves correspond to different values of the scaling parameter ℓ . The Fermi surface is divided in $M = 16$ patches. As the patch index increases from $n = 0$ to $n = 15$ around the Fermi surface, the angle θ increases from 0 to 2π .

For the case of a repulsive Hubbard interaction, $U_0 > 0$, we find in contrast to the attractive situation that the formally irrelevant terms play an important role. As the initial BCS couplings are all repulsive, Cooper pairing can only happen via coupling to the AF channels or via the non-logarithmic corrections to scaling coming from the formally irrelevant terms in the six-point functions. We again compare RG flows which include only the leading logarithmic corrections (diamonds) against those in which all subdominant contributions at one-loop order are included (circles) in Fig. 9 for the case $\mu = 10^{-4}$, that is, slightly away from half-filling. Though qualitatively similar, there is considerable quantitative difference. At this small doping, AF tendencies dominate in both cases. Upon further increasing the chemical potential, as mentioned above there is a crossover into the $d_{x^2-y^2}$ BCS regime. The crossover occurs much sooner when the subleading terms are included. Finally, at large doping the nesting of the Fermi surface is completely eliminated, and neither the AF nor the BCS channels show any strong divergences.

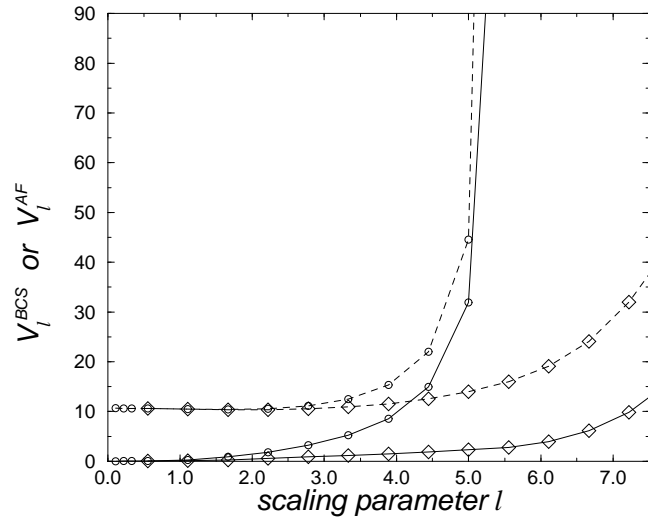


FIG. 9. Comparison of results obtained at one-loop level for the case of a repulsive Hubbard interaction and $\mu = 10^{-4}$. RG flows which include the effects of formally irrelevant terms (circles) are compared with RG flows for which only logarithmic contributions are retained (diamonds). Flow in the dominant BCS channel is depicted as a solid line and dominant AF sector is indicated by a dashed line.

C. Square Lattice With Next-Nearest-Neighbor Hopping ($t' \neq 0$)

Next we turn to the square lattice with added next-nearest-neighbor hopping amplitude t' along each of the two diagonal directions. Weak-coupling RG studies of this Hubbard model have been carried out previously by a number of groups^{24–26} using Salmhofer’s formulation^{22,23}. We have checked our calculation against these published results and find good agreement. The dispersion relation in this case is given by

$$\epsilon_{\mathbf{k}} = -2t_1(\cos k_x + \cos k_y) - 4t' \cos k_x \cos k_y \quad (9)$$

and Fig. 10 show the Fermi surface for the case $t_1 = -1$, $t' = 0.05$, and $\mu = 4t'$. The Fermi surface is centered around the Γ point ($\pm\pi, \pm\pi$) and van Hove singularities lie at the Fermi energy.

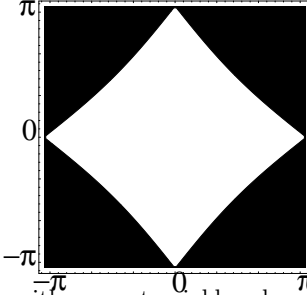


FIG. 10. Fermi surface of the square lattice with nearest-neighbor hopping $t_1 = -1$ and next-nearest-neighbor hopping $t' = 0.05$. The chemical potential $\mu = 4t'$.

This Fermi surface exhibits the $d_{x^2-y^2}$ superconducting instability. It is interesting to go a bit further and address the question of whether or not there is spontaneous time-reversal (\hat{T}) symmetry breaking with the appearance of an additional imaginary id_{xy} component to the superconducting order parameter. To answer this question we study the implications of RG flows which yield comparable attraction in two channels: one term with $d_{x^2-y^2}$ symmetry and a second with d_{xy} symmetry. A simple calculation of energetics then suffices to show that the two order parameters will phase-align as $d_{x^2-y^2} + id_{xy}$. The standard BCS equation yields a condensation energy of

$$\Delta E = E_{SC} - E_N = 2 \sum_{\mathbf{k} > \mathbf{k}_F} \left[\epsilon_{\mathbf{k}} - \frac{2\epsilon_{\mathbf{k}}^2 + \Delta_{\mathbf{k}}^2}{2\sqrt{\epsilon_{\mathbf{k}}^2 + \Delta_{\mathbf{k}}^2}} \right]. \quad (10)$$

For couplings V^{BCS} with comparable $d_{x^2-y^2}$ and d_{xy} components, the ansatz to maximize the condensation energy should be chosen to be $\Delta_{\mathbf{k}} = \Delta_{d_{x^2-y^2}}(\mathbf{k}) + u \Delta_{d_{xy}}(\mathbf{k})$, with u encoding information about the relative phase of the two components. Substituting this ansatz into Eq. 10, we may then determine the phase that maximizes the condensation energy ΔE . Fig. 11 shows the dependence of the integral

$$I(u) = \sum_{\mathbf{k} > \mathbf{k}_F} (2\epsilon_{\mathbf{k}}^2 + \Delta_{\mathbf{k}}^2) / \sqrt{\epsilon_{\mathbf{k}}^2 + \Delta_{\mathbf{k}}^2} \quad (11)$$

on the real part of u . The integral is maximized when u is purely imaginary ($\text{Re}\{u\} = 0$), hence the \hat{T} -breaking pairing symmetry $d_{x^2-y^2} + id_{xy}$ is the energetically favored. Physically this is reasonable, as this choice of the phase guarantees that a gap forms everywhere along the Fermi surface, lowering the ground-state energy.

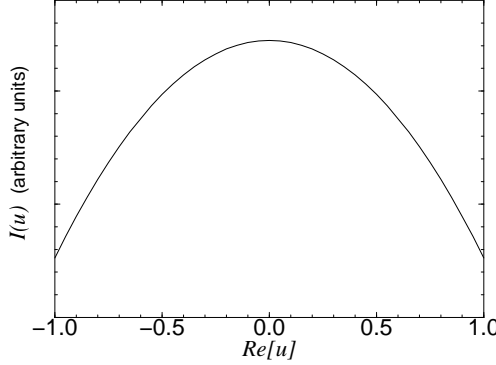


FIG. 11. Dependence of the integral $I(u)$ on the real part of u . The maximum of $I(u)$ occurs when $\text{Re}\{u\} = 0$, that is, when u is purely imaginary.

Returning to the square lattice, we find that upon integrating the RG equations for the case $t_1 = -1$, $t' = 0.05$ and $\mu = 4t'$, the dominant attractive BCS channel has $d_{x^2-y^2}$ symmetry as expected; see Fig. 12(A). A channel with d_{xy} symmetry also appears but it is repulsive in sign; see Fig. 12(B).

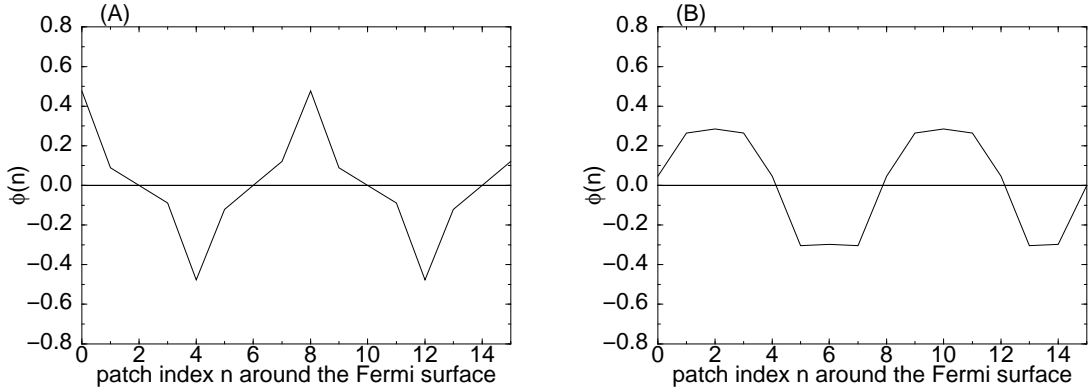


FIG. 12. Dominant BCS channels for the square lattice with $t_1 = -1$, $t' = 0.05$ and $\mu = 4t'$. The $d_{x^2-y^2}$ channel (A) is attractive while the d_{xy} channel (B) is repulsive. The absolute values of the eigenvalues are plotted in Fig. 13 as functions of the scaling parameter ℓ .

The strengths of each channel are plotted in Fig. 13 as a function of the scaling parameter ℓ . Since the d_{xy} channel is repulsive, no d_{xy} order will arise, and this may be taken as evidence against the formation of spontaneous time-reversal symmetry breaking of the $d_{x^2-y^2} + id_{xy}$ type.

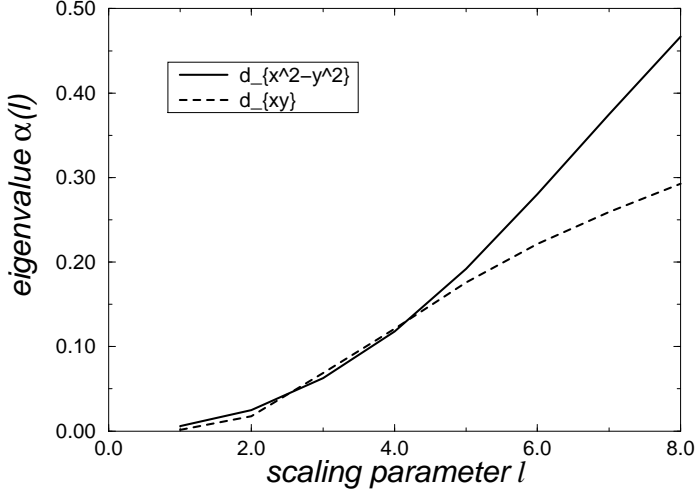


FIG. 13. Flow of the eigenvalues for the $d_{x^2-y^2}$ and d_{xy} channels shown in Fig. 12.

D. Towards the Triangular Lattice ($t_2 \neq 0$, $t_2 < t_1$)

Introducing non-zero t_2 along just one of the two diagonals, as shown in Fig. 1, offers a *different* way of breaking-up perfect nesting and enhancing BCS instabilities, even at half-filling.²⁷ For sufficiently large t_2 there is a crossover to a regime where the BCS processes eventually dominate, signaling a superconducting instability. Furthermore, because the Fermi surface is imperfectly nested, the growth of both BCS and AF couplings weakens. Further increasing t_2 eventually destroys nesting of the Fermi surface altogether and both types of divergences are suppressed. Three cases illustrating the crossover are shown in Fig. 14.

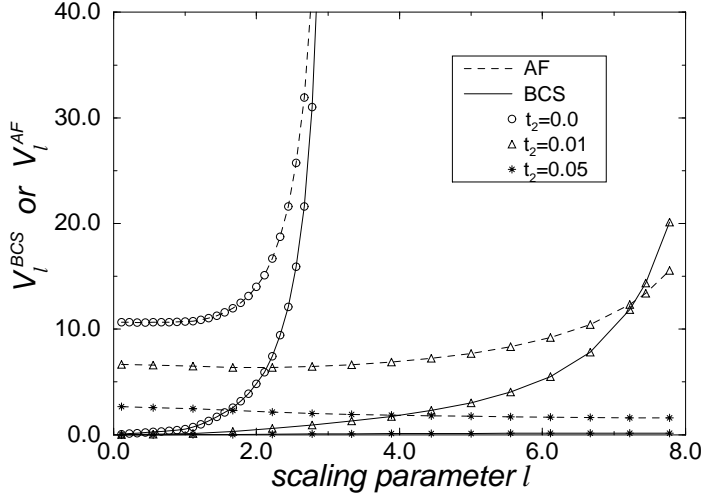


FIG. 14. At half-filling, spin-wave instability occurs for $t_2 = 0$, but as t_2 increases, there is a BCS instability wins over. This is due to imperfect nesting. As t_2 is increased further, the nesting is destroyed and both divergences are suppressed. The hopping t_1 is chosen such that $t_1 + t_2 = 1$.

As further increases in the diagonal hopping t_2 suppress the $d_{x^2-y^2}$ BCS channel, this channel diminishes relative to other subdominant BCS channel with different symmetries, for example d_{xy} - or p-wave, as shown in Fig. 15. These other channels, however, are all repulsive and hence do not lead to BCS instabilities by themselves.

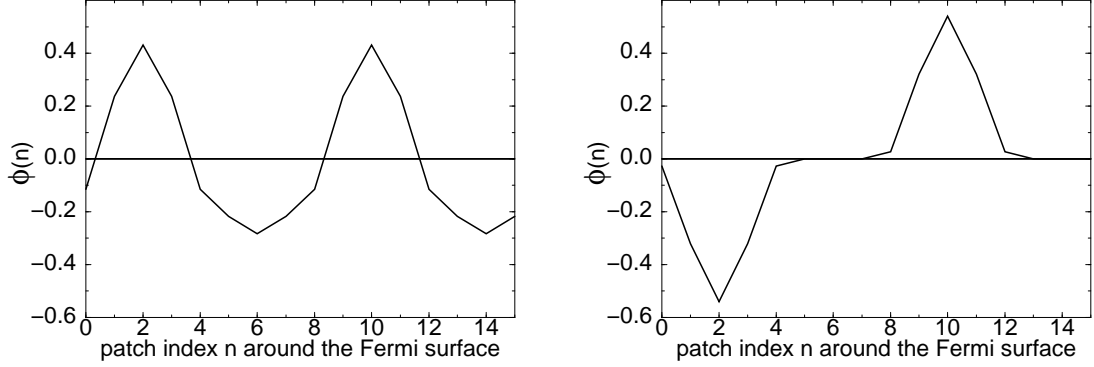


FIG. 15. Dominant BCS channels for $t_1 = 0.9$ and $t_2 = 0.1$, at half-filling and at scaling parameter $\ell = 5$. These channels are both repulsive (with eigenvalues of 0.781 and 0.648 respectively). The attractive $d_{x^2-y^2}$ BCS channel has a small eigenvalue of -0.268.

We note that the Hubbard model on the anisotropic triangular lattice has also been studied using the random-phase approximation²⁸ and the fluctuation-exchange (FLEX) approximation^{29–31}. The d -wave superconducting instability was found to be dominant for a large range of values of $t_2/(t_1 + t_2)$ interpolating between the square lattice and the isotropic triangular lattice.

E. Isotropic Triangular Lattice At Half-Filling

For the special case of the isotropic triangular lattice ($t_1 = t_2 = 0.5$) at half-filling, the weak-coupling RG flows do not show any BCS instabilities. The dominant BCS channels, $d_{x^2-y^2}$, d_{xy} and p , are all repulsive. These channels are depicted in Fig. 16(A), 16(B) and 16(C).

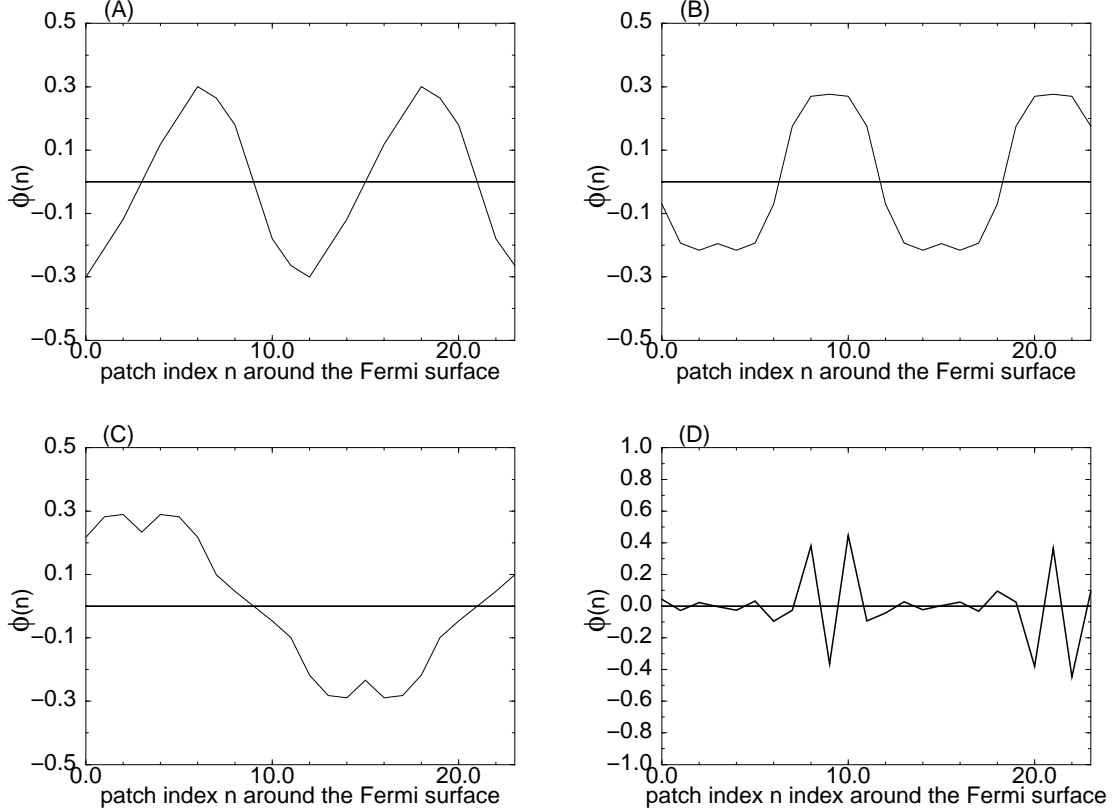


FIG. 16. BCS channels for the isotropic triangular lattice $t_1 = t_2 = 0.5$. Channels with $d_{x^2-y^2}$ (A), d_{xy} (B) and p (C) symmetries all appear as repulsive channels (with eigenvalues 0.185, 0.172 and 0.280, respectively). The largest attractive BCS channel is shown in (D), but it has a very small coefficient (-0.098) and the rapid oscillations suggest that the calculation is not accurate at this point. In the calculation, the Fermi surface was divided into $M = 24$ patches, instead of just 16, to improve the accuracy in the higher wave channels.

Fig. 16(D) shows the first attractive channel that develops, but the rapid oscillations in the effective potential, and its small size, indicate that the calculation is not reliable.

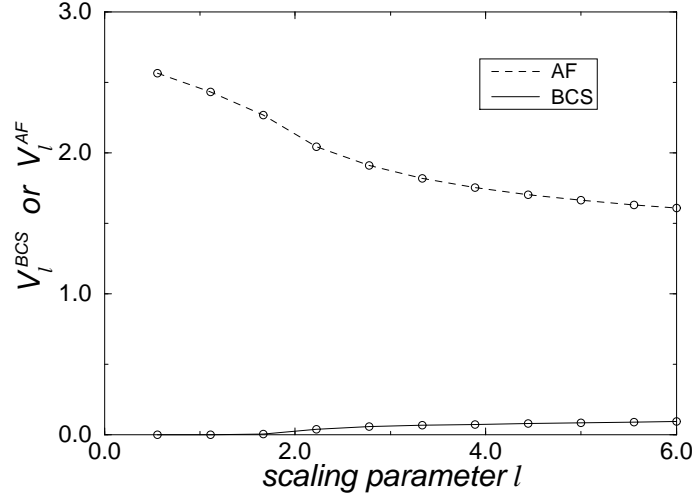


FIG. 17. Flow of dominant AF and BCS channels for the case of the isotropic triangular lattice.

In Fig. 17 the dominant AF and BCS channels are compared. Neither channel shows strong divergences, but the AF channel is significantly larger than the BCS channel. Thus there are signs of re-entrant antiferromagnetic long-range order. We speculate that there exist four different regions as the isotropy parameter $t_2/(t_1 + t_2)$ changes from 0 (square lattice) to 1 (decoupled chains). These phases are shown in Fig. 18. At $t_2 = 0$ the system exhibits long-range antiferromagnetic Néel order (LRO) with ordering vector $\vec{Q} = (\pi, \pi)$. But this long-range order is suppressed by turning on t_2 . Instead $d_{x^2-y^2}$ BCS instabilities dominate and only short-range order (SRO) occurs. Both AF and BCS instabilities are suppressed as t_2 is further increased and the nesting is completely eliminated. Nevertheless, the AF coupling remains significantly larger than the BCS coupling. In the strong-coupling limit $U \rightarrow \infty$ the model can be mapped onto a nearest-neighbor spin-1/2 Heisenberg antiferromagnet which of course is insulating. On the isotropic triangular lattice this antiferromagnet exhibits long-range AF order^{32,33} with ordering wave vector $\vec{Q} = (4\pi/3, 0)$. The question of whether or not our weak-coupling analysis can describe this strong-coupling limit is tantamount to asking whether or not one or more intermediate-coupling fixed points intervene between the repulsive weak-coupling fixed point that is accessible in our RG analysis, and the attractive strong-coupling fixed point which describes the antiferromagnetic insulator. Finally as t_2 becomes larger than t_1 , the chains begin to decouple. In the extreme limit of independent chains there can be no long-range spin order, as the Mermin-Wagner theorem tells us that continuous symmetries cannot break in 1+1 dimensions.

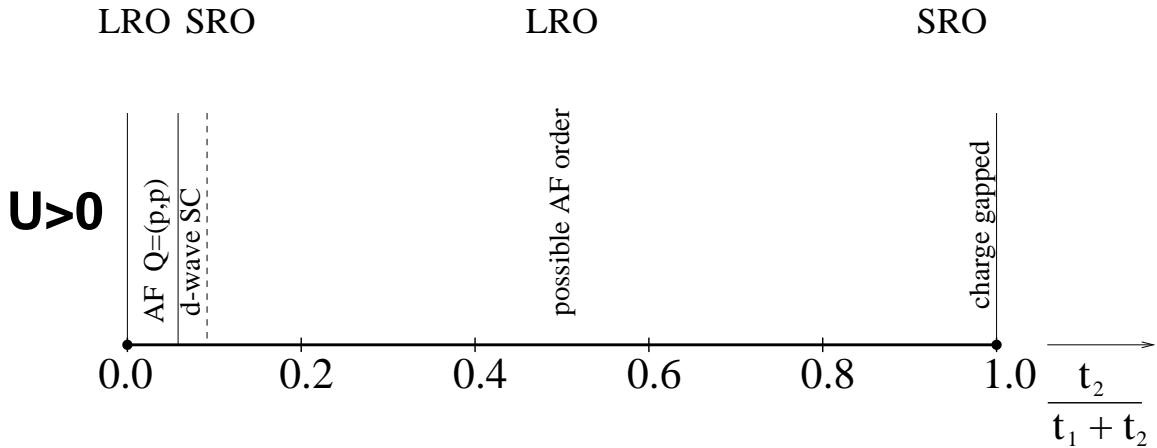


FIG. 18. Four regions (LRO-SRO-LRO-SRO) identified as $t_2/(t_1 + t_2)$ goes from 0 (square lattice) to 1 (decoupled chains).

Curiously, four such regions (LRO-SRO-LRO-SRO) have also been identified in the corresponding strong-coupling Heisenberg antiferromagnet with two exchange couplings J_1 and J_2 . The phase diagram of this model has been studied via a straightforward $1/S$ expansion^{34,35}, a series expansion method³⁶, and a large- N $\text{Sp}(N)$ solution³⁷. All three methods find two regions of long-range order: near the limit of a square lattice ($J_2 = 0$) and near the isotropic point ($J_2 = J_1$). It is remarkable that our weak-coupling RG analysis shows similar behavior.

The Hubbard model on the triangular lattice has been studied at intermediate values of the interaction strength within the Hartree-Fock approximation^{38,39} and within the slave-boson method⁴⁰⁻⁴². A Mott-Hubbard metal-insulator transition is found to occur at a relatively large value of U_c ($U_c = 5.27t$ for the Hartree-Fock calculation³⁸ and $U_c = 7.23t$ or $7.68t$ from the slave-boson calculations^{40,42}). At a smaller value of $U = U_{c1}$ there is also a continuous transition from a paramagnetic metallic phase to a metallic phase with incommensurate spiral order. The Hartree-Fock calculation yields $U_{c1} = 3.97t$ and the slave-boson calculation gives $U_{c1} = 6.68t$ for this transition. Signs of re-entrant AF order in our weak-coupling RG calculation, namely the relatively large size of the AF channels in comparison with the BCS channels, are broadly consistent with this picture, as AF tendencies can be a precursor to a transition to the insulating state.

IV. CONCLUSION

Hubbard models have received extensive study in the context of high- T_c superconductivity. We have reproduced the well-known result that there is an AF instability at half-filling on the square lattice with repulsive on-site Coulomb interaction and nearest-neighbor hopping. Furthermore, upon doping the system away from half filling, a crossover to a BCS regime with $d_{x^2-y^2}$ pairing symmetry occurs as expected. We have shown that it is important to retain subleading, formally irrelevant, corrections to the RG flows when the bare interaction is repulsive and the Fermi surface is nearly nested. More important, we have shown another way of triggering a BCS instability. Keeping the system at half filling, but introducing the diagonal hopping t_2 as shown in Fig. 1 along one of the two diagonals, breaks up perfect nesting. Corresponding magnetic frustration kills the spin-density wave, and Cooper pairing dominates, at least if t_2 is not too large. This result suggests that superconductivity can occur in a model of strongly correlated electrons, even at half-filling. We emphasize that stripes are not expected to play a role here; even moderate on-site Coulomb repulsion should inhibit charge segregation at half-filling.

The half-filled Hubbard model on the anisotropic triangular lattice has been proposed as a minimal description of the conducting layers of the $\kappa - (\text{BEDT-TTF})_2X$ organic superconductors. It is important to establish the pairing symmetry of the superconducting state of these materials. Our theoretical results predict pairing of the $d_{x^2-y^2}$ type and signs of such order have been seen experimentally. We did not find any evidence of spontaneous time-reversal symmetry breaking. Pairing symmetry of the type $d_{x^2-y^2} \pm id_{xy}$ would occur if an attractive d_{xy} channel arose in addition to the $d_{x^2-y^2}$ channel. We find that attractive d_{xy} channels neither occur when next-nearest-neighbor hopping t' is included on the square lattice, nor when non-zero hopping t_2 is turned on along one of the two diagonal directions. Finally, we made contact with previous work on Heisenberg antiferromagnets on the anisotropic triangular lattice. Our weak-coupling RG calculation shows AF tendencies in two separate regimes – tendencies which seem to correspond with the two AF ordered phases seen at large- U .

Acknowledgments We thank Tony Houghton, Ross McKenzie, Chung-Hou Chung and Matthias Vojta for useful

discussions. This work was supported in part by the NSF under Grant No. DMR-9712391.

- ¹ J. M. Williams *et al.*, *Organic superconductors (including fullerenes): synthesis, structure, properties, and theory*, (Prentice Hall, Englewood Cliffs, 1992).
- ² T. Ishiguro and K. Yamaji, *Organic Superconductors*, Second edition (Springer-Verlag, Berlin, 1997).
- ³ R. H. McKenzie, *Comments Cond. Mat. Phys.* **18**, 309 (1998).
- ⁴ R. H. McKenzie, *Science* **278**, 820 (1997).
- ⁵ S. M. De Soto, C. P. Slichter, A. M. Kini, H. H. Wang, U. Geiser and J. M. Williams, *Phys. Rev. B* **52**, 10364 (1995)
- ⁶ K. Kanoda, K. Miyagawa, A. Kawamoto and Y. Nakazawa, *Phys. Rev. B* **54**, 76 (1996).
- ⁷ Y. Nakazawa and K. Kanoda, *Phys. Rev. B* **55**, R8670 (1997).
- ⁸ A. Carrington, I. J. Bonalde, R. Prozorov, R. W. Giannetta, A. M. Kini, J. Schlueter, H. H. Wang, U. Geiser and J. M. Williams, *Phys. Rev. Lett.* **83**, 4172 (1999).
- ⁹ M. Pinterić, S. Tomić, M. Prester, D. Drobac, O. Milat, K. Maki, D. Schweitzer, I. Heinen and W. Strunz, *Phys. Rev. B* **61**, 7033 (2000).
- ¹⁰ M. Lang, N. Toyota, T. Sasaki and H. Sato, *Phys. Rev. Lett.* **69**, 1443 (1992).
- ¹¹ D. R. Harshman, A. T. Fiory, R. C. Haddon, M. L. Kaplan, T. Pfiz, E. Koster, I. Shinkoda and D. Ll. Williams, *Phys. Rev. B* **49**, 12990 (1994).
- ¹² M. Dressel, O. Klein, G. Grüner, K. D. Carlson, H. H. Wang and J. M. Williams, *Phys. Rev. B* **50**, 13603 (1994).
- ¹³ H. Elsinger, J. Wosnitza, S. Wanka, J. Hagel, D. Schweitzer and W. Strunz, *Phys. Rev. Lett.* **84**, 6098 (2000).
- ¹⁴ S. Lefebvre, P. Wzietek, S. Brown, C. Bourbonnais, D. Jérôme, C. Mézière, M. Fourmigué and P. Batail, “*Mott transition, antiferromagnetism, and unconventional superconductivity in layered organic superconductors*,” cond-mat/0004455.
- ¹⁵ H. Kino and H. Fukuyama, *J. Phys. Soc. Jpn.* **65**, 2158 (1996).
- ¹⁶ E. H. Lieb and F. Y. Wu, *Phys. Rev. Lett.* **20**, 1145 (1968).
- ¹⁷ E. S. Choi, J. S. Brooks, S. Y. Han, L. Balicas and J. S. Qualls, “*Transverse and in-plane modification of superconductivity and electronic structure in the quasi-two dimensional organic conductor $\kappa-(BEDT-TTF)_2Cu(SCN)_x$ by uniaxial stress*,” cond-mat/0008348.
- ¹⁸ D. Zanchi and H. J. Schulz, *Europhys. Lett.* **44**, 235 (1998); *Phys. Rev. B* **61**, 13609 (2000).
- ¹⁹ See, for example, A. Houghton, H.-J. Kwon, and J. B. Marston, *Adv. Phys.* **49**, 141 (2000) and references therein.
- ²⁰ R. Shankar, *Rev. Mod. Phys.* **66**, 129 (1994).
- ²¹ D. Zanchi and H. J. Schulz, *Phys. Rev. B* **54**, 9509 (1996).
- ²² M. Salmhofer, *Comm. Math. Phys.* **194**, 249 (1998).
- ²³ M. Salmhofer, *Renormalization: An Introduction*, (Springer-Verlag, Berlin, 1999).
- ²⁴ C. J. Halboth and W. Metzner, *Phys. Rev. B* **61**, 7364 (2000).
- ²⁵ C. J. Halboth and W. Metzner, “*d-wave superconductivity and Pomeranchuk instability in the two-dimensional Hubbard model*,” cond-mat/0003349.
- ²⁶ C. Honerkamp, M. Salmhofer, N. Furukawa and T. M. Rice, “*Breakdown of the Landau-Fermi liquid in two dimensions due to Umklapp scattering*,” cond-mat/9912358.
- ²⁷ S.-W. Tsai and J. B. Marston, “ *$\kappa-(BEDT-TTF)_2X$ organic crystals: superconducting versus antiferromagnetic instabilities in an anisotropic triangular lattice Hubbard model*,” to appear in *Can. J. Phys.* (2000).
- ²⁸ M. Vojta and E. Dagotto, *Phys. Rev. B* **59**, R713 (1999).
- ²⁹ H. Kondo and T. Moriya, *J. Phys. Soc. Jpn.* **67**, 3695 (1998).
- ³⁰ H. Kino and K. Kontani, *J. Phys. Soc. Jpn.* **67**, 3691 (1998).
- ³¹ J. Schmalian, *Phys. Rev. Lett.* **81**, 4232 (1998).
- ³² R. R. P. Singh and D. Huse, *Phys. Rev. Lett.* **68**, 1766 (1992).
- ³³ B. Bernu, P. Lecheminant, C. Lhuillier and L. Pierre, *Phys. Rev. B* **50**, 10048 (1994).
- ³⁴ J. Merino, R. H. McKenzie, J. B. Marston and C.-H. Chung, *J. Phys. C* **11**, 2965 (1999).
- ³⁵ A. E. Trumper, *Phys. Rev. B* **60**, 2987 (1999).
- ³⁶ Z. Weihong, R. H. McKenzie and R. R. P. Singh, *Phys. Rev. B* **59**, 14367 (1999).
- ³⁷ C. H. Chung, J. B. Marston and R. H. McKenzie, unpublished.
- ³⁸ H. R. Krishnamurthy, C. Jayaprakash, S. Sarker and W. Wenzel, *Phys. Rev. Lett.* **64**, 950 (1990).
- ³⁹ C. Jayaprakash, H. R. Krishnamurthy, S. Sarker and W. Wenzel, *Europhys. Lett.* **15**, 625 (1991).
- ⁴⁰ C. J. Gazza, A. E. Trumper and H. A. Ceccato, *J. Phys. C* **6**, L625 (1994).
- ⁴¹ A. Feiguin, C. J. Gazza, A. E. Trumper and H. A. Ceccato, *J. Phys. C* **9**, L27 (1997).
- ⁴² M. Capone, L. Capriotti, F. Becca and S. Caprara, “*The Mott metal-insulator transition in the half-filled Hubbard model on the triangular lattice*,” cond-mat/0006437.